Influence of Magnetofossils on Paleointensity Estimations Inferred From Principal Component Analyses of First-Order Reversal Curve Diagrams for Sediments From the Western Equatorial Pacific

Geochemistry, Geophysics, Geosystems®

AGU ADVANCING EARTH AND SPACE SCIENCE

RESEARCH ARTICLE
10.1029/2021GC010081

Key Points:

- Principal component analyses were applied to first-order reversal curve diagrams from three sediment cores in western equatorial Pacific
- Relative paleointensity (RPI; natural remanent magnetization/anhysteretic remanent magnetization [ARM]) decreases with increasing proportion of magnetofossils due to their higher ARM acquisition efficiency
- Bending and collapse of biogenic magnetite chains may also influence ARM susceptibility to saturation isothermal remanent magnetization ratio and RPI estimation

Supporting Information:

Supporting Information may be found in the online version of this article.

Correspondence to:

T. Yamazaki,
yamazaki@aori.u-tokyo.ac.jp

Citation:

Inoue, K., Yamazaki, T., & Usui, Y. (2021). Influence of magnetofossils on paleointensity estimations inferred from principal component analyses of first-order reversal curve diagrams for sediments from the western equatorial Pacific. *Geochemistry, Geophysics, Geosystems*, *22*, e2021GC010081. https://doi.org/10.1029/2021GC010081

Received 5 AUG 2021
Accepted 6 OCT 2021

Influence of Magnetofossils on Paleointensity Estimations Inferred From Principal Component Analyses of First-Order Reversal Curve Diagrams for Sediments From the Western Equatorial Pacific

Kosuke Inoue[1], Toshitsugu Yamazaki[1], and Yoichi Usui[2]

[1]Atmosphere and Ocean Research Institute, The University of Tokyo, Kashiwa, Japan, [2]Volcanoes and Earth's Interior Research Center, Research Institute for Marine Geodynamics, Japan Agency for Marine-Earth Science and Technology, Yokosuka, Japan

Abstract Relative abundance of magnetite originated from magnetotactic bacteria (magnetofossils) in sediments may influence relative paleointensity (RPI) estimations of the geomagnetic field, as some studies reported an inverse correlation between RPI and the ratio of anhysteretic remanent magnetization susceptibility to saturation isothermal remanent magnetization (k_{ARM}/SIRM), a proxy of the proportion of biogenic to terrigenous magnetic minerals as well as magnetic grain size. This study aims to evaluate the influence of magnetofossils on RPI estimations more selectively using first-order reversal curve (FORC) diagrams. We studied three cores (KR0515-PC4, MD982187, and MR1402-PC1) from the western equatorial Pacific, among which large differences exist in the average natural remanent magnetization intensity normalized by ARM and k_{ARM}/SIRM. Principal component analyses (PCAs) were applied to FORC diagrams measured on bulk specimens from the three cores and silicate-hosted magnetic inclusions extracted from Core MD982187, and three endmembers (EMs) were revealed (EM1: silicate-hosted magnetic inclusions, EM2: other terrigenous, EM3: biogenic). EM3 proportions vary widely among the three cores. The average RPI decreases with increasing EM3 proportion, which is probably caused by higher ARM acquisition efficiency of magnetofossils due to small magnetostatic interactions. EM3 proportion correlates with k_{ARM}/SIRM, which confirms that k_{ARM}/SIRM represents the proportion of biogenic to terrigenous magnetic components. Core MR1402-PC1 has the highest EM3 proportion, and its within-core variation is small. From FORC-PCA applied solely to this core, we infer that the configurations of biogenic magnetite chains such as bending and collapse may also influence k_{ARM}/SIRM and RPI estimations.

Plain Language Summary Information on the variations of the geomagnetic field intensity in the past (relative paleointensity [RPI]) is important for understanding, for example, how the geomagnetic field is generated in the Earth's core and whether the geomagnetic field has been related to evolution of life. Marine sediments potentially preserve continuous records of RPI, but it has been suspected that magnetic-mineral composition changes of sediments may induce artificial RPI changes. This study aims to evaluate the influence of fossil magnetite produced by magnetotactic bacteria on paleointensity estimations. We used a technique based on magnetic hysteresis for estimating the proportion of biogenic magnetite to other terrigenous magnetic minerals in magnetic mineral assemblages, which was applied to sediment cores taken from the western equatorial Pacific. This technique enables to focus more on biogenic magnetite compared with previous estimations using a magnetic proxy. We confirmed that apparent RPI values inversely correlate with the proportion of the biogenic to terrigenous magnetic components, which implies that RPI is underestimated at a higher biogenic magnetite proportion. In addition, degradation of chain arrangements of magnetite originally produced by magnetotactic bacteria may also influence RPI. Our results will be useful for improving the reliability of paleointensity estimations.

1. Introduction

Information on geomagnetic paleointensity is fundamentally important for better understanding of the behavior and mechanism of the geodynamo, and marine sediments potentially provide continuous records

of paleointensity variations (e.g., Tauxe & Yamazaki, 2015). Relative paleointensity (RPI) estimations from sediments are usually based on the normalization of natural remanent magnetization (NRM) intensity with the intensity of laboratory induced remanent magnetization for compensating changes of "magnetizability" within the target sediments (Johnson et al., 1948; Tauxe, 1993). As no artificial remanent magnetization perfectly represents magnetizability, that is, the efficiency of depositional remanent magnetization acquisition, successful RPI estimations were derived from sediments with relatively uniform magnetic properties in general. For the normalizer, anhysteretic remanent magnetization (ARM) has often been used mainly because unlike to isothermal remanent magnetization (IRM), ARM is not sensitive to multi-domain (MD) magnetic grains, which do not carry stable NRM (King et al., 1983; Levi & Banerjee, 1976).

Magnetic mineral assemblages in sediments are usually a mixture of magnetic minerals of different origins such as magnetite originated from magnetotactic bacteria (magnetofossils), terrigenous magnetic minerals, and silicate-hosted magnetic inclusions, and each is thought to have a different paleomagnetic recording efficiency (Chang et al., 2016; L. Chen et al., 2017; Yamazaki et al., 2013). It has become recognized that magnetofossils are ubiquitous in marine sediments, and magnetofossils were often revealed to be the major constituent of magnetic mineral assemblages in deep-sea sediments (Roberts et al., 2011, 2012; Yamazaki & Ikehara, 2012; Yamazaki & Shimono, 2013). Variations in the proportion of magnetofossils to terrigenous magnetic minerals can be estimated from the ratio of ARM susceptibility to saturation IRM (k_{ARM}/SIRM) for deep-sea sediments in pelagic environments (Egli, 2004; Yamazaki, 2008; Yamazaki et al., 2013, 2020), in which magnetic grain-size changes, another control factor of the k_{ARM}/SIRM ratio (Banerjee et al., 1981; King et al., 1982), are considered to be small because of a long distance from terrigenous source regions. Some deep-sea sediment cores showed an inverse correlation between RPI and the k_{ARM}/SIRM ratio, which raised a concern that changing amounts of magnetofossils in sediments may influence and contaminate RPI estimations (Hoffmann & Fabian, 2009; Sakuramoto et al., 2017; Yamazaki & Yamamoto, 2018; Yamazaki et al., 2013). However, interpretation of the k_{ARM}/SIRM ratio has inherent ambiguity; the ratio responds to both magnetostatic interactions and magnetic grain size. Thus it is difficult to quantitatively evaluate the amount of magnetofossils from the k_{ARM}/SIRM ratio.

In this study, we aim to evaluate the possible influence of magnetofossils on RPI estimations more selectively. For this purpose, we use first-order reversal curve (FORC) diagrams. FORC diagrams have become used widely to detect magnetofossils based on its uniaxial single-domain (SD) behavior with little magnetostatic interactions (Chang et al., 2014; A. P. Chen et al., 2007; Egli et al., 2010; Li et al., 2012; Yamazaki, 2008). By applying principal component analysis (PCA) to FORC diagrams (Harrison et al., 2018; Lascu et al., 2015), it is possible to estimate quantitatively the proportion of magnetization carried by magnetofossils (Channell et al., 2016; Roberts et al., 2018; Yamazaki et al., 2020). It is considered that the FORC-PCA method can reduce the ambiguity of magnetofossil proportion estimations compared with the k_{ARM}/SIRM ratio. Furthermore, information on bending and/or collapse of biogenic magnetite chains in sediments and differences in the morphology of biogenic magnetite can also be obtained from FORC diagrams (Berndt et al., 2020; Chang et al., 2019; Usui & Yamazaki, 2021; Wagner et al., 2021; Yamazaki et al., 2020), which may also influence RPI estimations. In this study, we use three sediment cores taken from the western equatorial Pacific, in which large differences in the proportion of magnetofossils to terrigenous magnetic minerals are expected. Based on the results of FORC-PCA, we show increased underestimation of RPI normalized by ARM with increasing relative abundance of magnetofossils. We also discuss the possible influence of biogenic magnetite chain configurations on RPI estimations.

2. Studied Cores and Background

Three piston cores, KR0515-PC4, MD982187, and MR1402-PC1, collected from the West Caroline Basin in the western equatorial Pacific were used in this study (Figure 1). The positions and water depths of these sites are presented in Table 1. Terrigenous particles in this region are considered to be mainly of fluvial origin (Dang et al., 2020; Wu et al., 2013). Riverine input mainly from the Sepik River in the northern part of New Guinea is delivered to this region by the New Guinea Coastal Undercurrent and Equatorial Under Current. The contribution of eolian dust is small in this region (Rea, 1994; Winckler et al., 2016; Wu et al., 2013). Sediments in this area are expected to be suitable for examining the influence of proportional changes in the magnetofossil and terrigenous magnetic components on RPI estimations because it

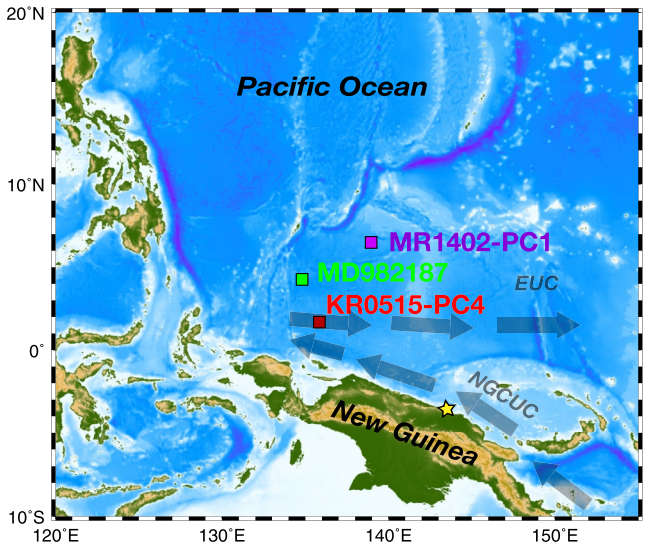

Figure 1. Map of the western equatorial Pacific and locations of the studied cores. Arrows show the New Guinea Coastal Undercurrent (NGCUC) and Equatorial Undercurrent (EUC) that deliver fluvial sediment particles in this region (after Dang et al., 2020). Star indicates the location of the mouth of the Sepik River.

is expected that the proportion of the terrigenous magnetic component varies depending on the distance from New Guinea.

Core KR0515-PC4 consists of greenish gray hemipelagic clay and contains a minor amount of foraminifera (Yamazaki & Horiuchi, 2016). This is one of the four cores used for constructing a stacked RPI curve for the last 400 kyr in the West Caroline Basin (Yamazaki et al., 2008). Core MD982187 consists mainly of hemipelagic clay with calcareous and siliceous microfossils. RPI variations of the last 3 m.y. estimated from this core were published in Yamazaki and Oda (2005). Core MR1402-PC1 consists of light gray calcareous ooze and light brownish gray to grayish yellow brown clayey calcareous ooze. A continuous RPI record from 0.6 to 3.2 Ma was successfully recovered from the core (Sakuramoto et al., 2017). Sedimentation rates of these cores (Table 1) decrease with increasing distance from New Guinea. In Core KR0515-PC4, which is the closest to New Guinea, the average sedimentation rate is about 38 m/m.y. In Core MD982187, sedimentation rates vary from 5 to 20 m/m.y. with an upcore increasing trend. In Core MR1402-PC1, sedimentation rates are 4–5.5 m/m.y. in the most part of the core.

The average RPI estimated from normalizing NRM intensity with ARM intensity differs among the three cores, in particular between Core MR1402-PC1 and the other two cores (Figure 2a). Although the age intervals of the individual paleointensity records are not the same, the time-averaged paleointensity of the geomagnetic field did not vary significantly within the last ca. 3 m.y. (Channell et al., 2009; Yamazaki & Yamamoto, 2018). We thus infer that the difference in the average normalized intensities among the three cores originates from difference in acquisition efficiency of NRM and/or ARM, and that the different efficiencies are caused by variations in magnetic mineral composition as well as other sediment properties among these cores. The average normalized intensity inversely correlates with the k_{ARM}/SIRM ratio (Figure 2a, Table 2). Normalized intensity is the highest in Core KR0515-PC4 and the lowest in Core MR1402-PC1, whereas the k_{ARM}/SIRM ratio is the lowest in the former core and the highest in the latter core. A weak inverse correlation is also observed within individual cores, in particular in Core MR1402-PC1 (insets of Figure 2a). The k_{ARM}/SIRM ratio has been used as a proxy of magnetic grain size (Banerjee et al., 1981; King et al., 1982). As ARM acquisition efficiency increases with decreasing magnetostatic interactions among magnetic grains, and thus the k_{ARM}/SIRM ratio reflects the proportion of magnetofossils in pelagic environments where magnetic grain size (domain state) change is considered to be small (Egli, 2004; Yamazaki, 2008; Yamazaki et al., 2013, 2020). The occurrence of magnetofossils in these cores was confirmed by transmission electron microscopy (Core KR0515-PC4: Yamazaki & Horiuchi, 2016, Core MD982187: Yamazaki, 2017, Core MR1402-PC1: Sakuramoto et al., 2017).

When NRM intensity is normalized by IRM, the normalized intensity still shows differences among the cores, in particular between Core KR0515-PC4 and the other two cores, although the magnitude of the differences is smaller than in the case of ARM normalization (Figure 2b). Within individual cores, Core MR1402-PC1 shows a weak inverse correlation with the k_{ARM}/SIRM ratio (Figure 2b). These observations suggest that RPI estimations normalized by IRM are also influenced by changes in the relative abundance of magnetofossils and terrigenous magnetic minerals when the changes are large.

Table 1
Information of the Cores Used in This Study

Core ID	Latitude (N)	Longitude (E)	Water depth (m)	Sedimentation rate (m/m.y.)	Reference
KR0515-PC4	1°42.71′	135°50.87′	4,277	38	1, 2
MD982187	4°15.98′	134°49.11′	4,623	5–20	3, 4
MR1402-PC1	6°29.99′	138°56.51′	3,855	4–5.5	5

Note. References: 1: Yamazaki et al. (2008), 2: Yamazaki and Horiuchi (2016), 3: Yamazaki and Oda (2005), 4: Tauxe and Yamazaki (2015), 5: Sakuramoto et al. (2017).

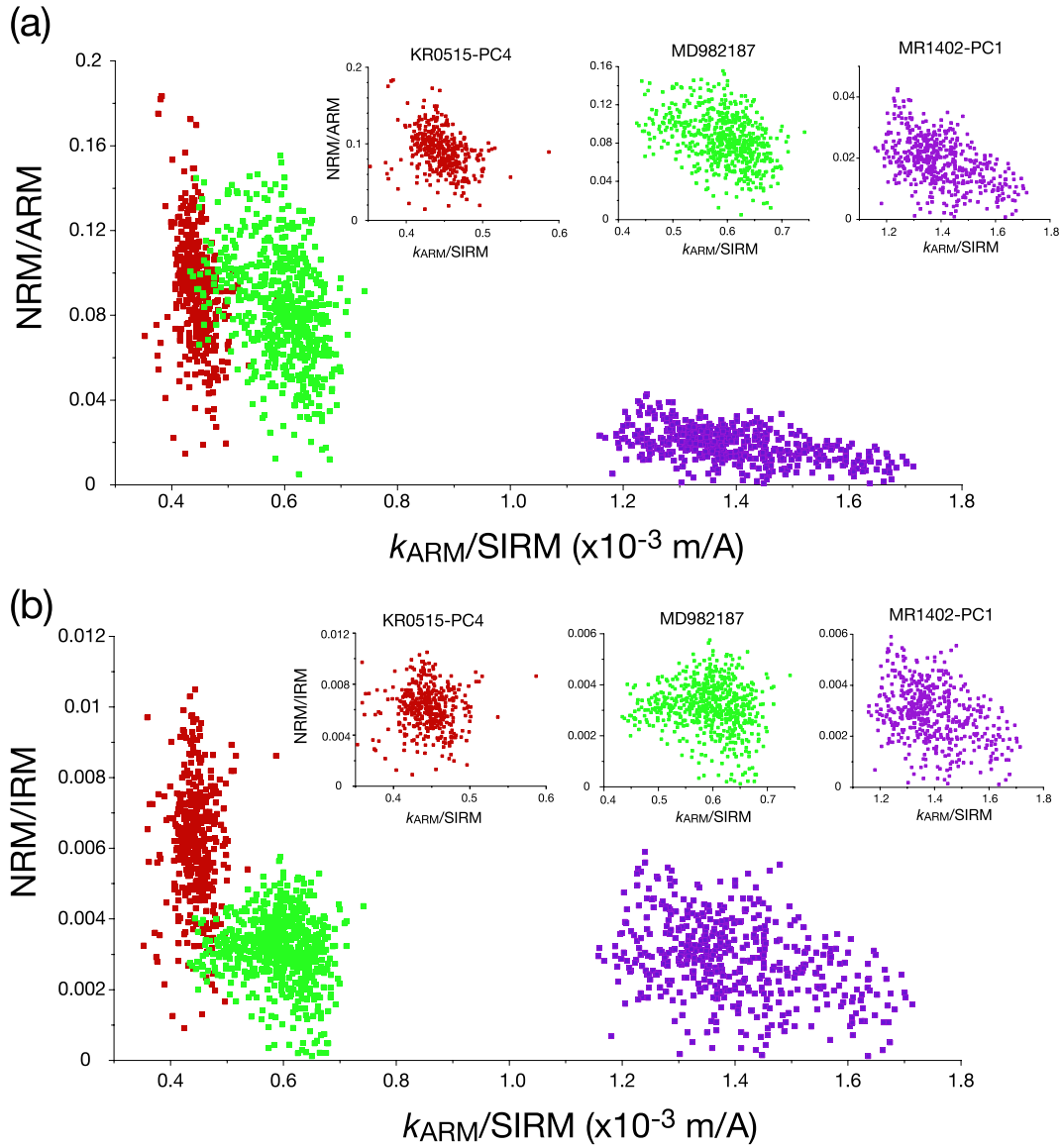

Figure 2. Relation between relative paleointensity based on natural remanent magnetization (NRM) intensity normalized by anhysteretic remanent magnetization (ARM) (a) or isothermal remanent magnetization (IRM) (b) intensities and the ARM susceptibility to saturation IRM (k_{ARM}/SIRM) ratio for Cores KR0515-PC4 (red), MD982187 (green), and MR1402-PC1 (purple). The insets show the plots of individual cores with the aspect ratios close to one. The data sets used were presented in the references listed in Table 1, except for NRM intensity normalized by IRM of Core KR0515-PC4. The normalized intensities of Cores KR0515-PC4 and MD982187 were calculated as NRM and ARM (or IRM) intensities after AF demagnetization at 30 mT, and those of Core MR1402-PC1 were from NRM versus ARM (or IRM) slopes of stepwise AF demagnetization.

In the following, we evaluate the contribution of magnetofossils in the three cores more selectively using FORC diagrams, and discuss their influence on RPI estimations focusing mainly on those normalized by ARM.

3. Methods

3.1. FORC Diagrams

FORC diagrams have become widely used as a method for characterizing quantitatively the constituents in magnetic mineral assemblages. On FORC diagrams, the distributions of coercivity (B_c) and magnetostatic interactions (B_u) are mapped, from which information on domain states, grain sizes and shapes, and mineralo-

Table 2
Relative Paleointensity (RPI) and Magnetic Properties of the Studied Cores

Core ID	RPI (NRM/ARM)	k_{ARM}/SIRM (10^{-3} m/A)	EM3 (biogenic) proportion (%)
KR0515-PC4	0.10 ± 0.02	0.44 ± 0.03	8.4 ± 1.9
MD982187	0.065 ± 0.018	0.59 ± 0.06	24.8 ± 6.0
MR1402-PC1	0.017 ± 0.008	1.40 ± 0.12	72.9 ± 2.9

Note. Mean and standard deviation (1σ) are presented. ARM, anhysteretic remanent magnetization; EM, endmember; k_{ARM}/SIRM, ARM susceptibility to saturation isothermal remanent magnetization; NRM, natural remanent magnetization.

gy of magnetic grains, and their spatial distributions can be obtained (Pike et al., 1999; Roberts et al., 2000, 2014). An assemblage of noninteracting SD grains produces a narrow peak elongated along the B_c axis at zero interaction field ($B_u = 0$) on the diagram, which is called the "central ridge." Intact biogenic magnetite chains in sediments are expected to behave as isolated noninteracting SD grains, and hence it is considered that the central ridge is diagnostic of magnetofossils in sediments (Chang et al., 2014; A. P. Chen et al., 2007; Egli et al., 2010; Li et al., 2012; Yamazaki, 2008). Magnetic grains of terrigenous origin tend to form aggregates in transport and deposition processes, and thus should have significant magnetostatic interactions. This yields a large vertical spread in the direction of the B_u axis on FORC diagrams, and hence terrigenous magnetic grains can be discriminated from magnetofossils (Channell et al., 2016; Roberts et al., 2012; Yamazaki & Ikehara, 2012; Yamazaki et al., 2020). Combined with micromagnetic simulations, it was recently revealed that the conditions of biogenic magnetite chains including chain bending and collapse, distance between biogenic magnetites in a chain, and the number of magnetite in a chain significantly influence the distributions of coercivity and magnetostatic interactions (Berndt et al., 2020; Chang et al., 2019).

FORC measurements were conducted using an alternating-gradient magnetometer (Princeton MicroMag 2900) at the Atmosphere and Ocean Research Institute, The University of Tokyo. Dried samples were cut to suitable sizes (tens of milligrams) and stuck to a probe with silicone grease. A total of 165 FORCs were measured, with B_c between 0 and 100 mT, B_u between −50 and 50 mT, and a field spacing of 1.3 mT. The maximum applied field was 1.0 T, and the averaging time for each measurement point was 200 ms. The numbers of samples measured were 48, 36, and 23 for Cores KR0515-PC4, MD982187, and MR1402-PC1, respectively.

FORCinel software (Harrison & Feinberg, 2008, version 3.06 in 2021) was used for the analyses. The VARIFORC algorithm of Egli (2013) was used for smoothing ($S_{c0} = 10$, $S_{b0} = 5$, $S_{c1} = S_{b1} = 10$, horizontal and vertical lamda = 0.2), which provides smaller smoothing in regions near $B_u = 0$ and larger smoothing for other regions. PCA was applied to the FORC data set to unmix magnetic components into a linear combination of endmembers (EMs) (Harrison et al., 2018; Lascu et al., 2015). The resolution of PCA grids was set to be 2 mT.

3.2. Silicate-Hosted Magnetic Inclusions

Recently it has been recognized that silicate-hosted magnetic inclusions are widely distributed in marine sediments, and potentially carry NRM (Chang et al., 2016; Usui et al., 2018; Zhang et al., 2018). To evaluate the contribution of silicate-hosted magnetic inclusions to the magnetization of the sediments in this region, we conducted chemical separation of quartz and feldspar from three samples of Core MD982187.

The samples were first treated with 1 N HCl in order to dissolve all carbonates and unprotected magnetic minerals including magnetofossils. Then, sodium pyrosulfate ($Na_2S_2O_7$) fusion technique was applied to separate quartz and feldspars from these samples (Blatt et al., 1982; Clayton et al., 1972; Stevens, 1991; Syers et al., 1968; Usui et al., 2018). Samples were first freeze-dried and heated up gradually to 460°C with $Na_2S_2O_7$ and then treated with 3 N HCl and washed with purified water. Next, the residues were heated to 50°C in 1 M NaOH overnight and washed with purified water. Finally, the residues were freeze-dried.

It is considered that only magnetic minerals remaining in the residues after all the above-mentioned procedures are inclusions in quartz and feldspar. SIRM imparted at a 2.5 T field with a pulse magnetizer was measured before and after the extraction using a spinner magnetometer. FORC measurements were conducted using the same parameters as the untreated samples mentioned above.

4. Results

All FORC diagrams from the three cores show the central ridge feature, indicative of noninteracting SD grains (Figure 3). This is considered to represent mainly biogenic magnetite chains because it is considered that terrigenous magnetic minerals tend to form aggregation and hence have strong magnetostatic

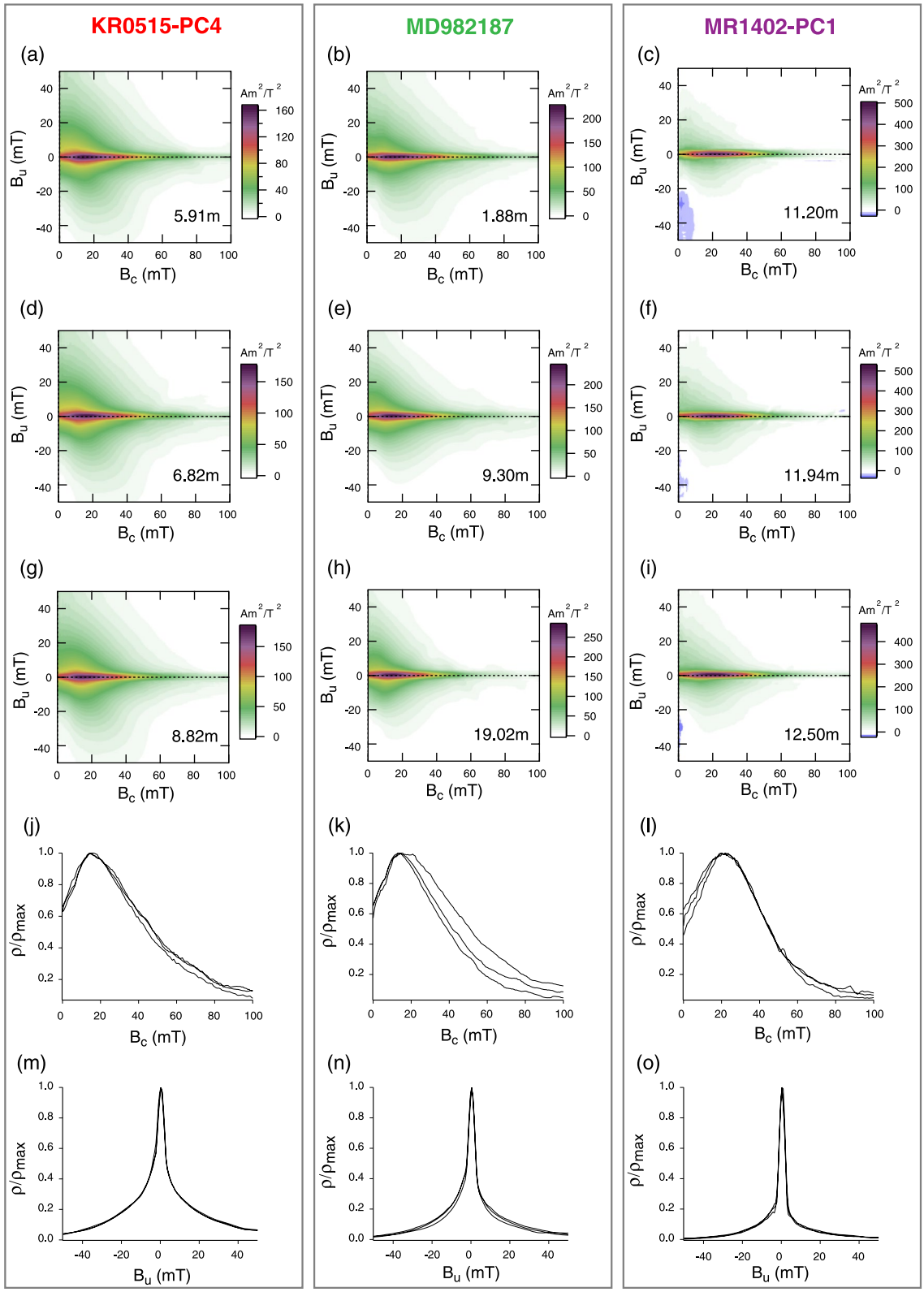

Figure 3. Examples of first-order reversal curve (FORC) diagrams measured on samples from the three cores. (a–i) FORC diagrams, (j–l) horizontal profiles along $B_u = 0$ mT of the three FORC diagrams presented above for individual cores, and (m–o) vertical profiles along $B_c = 20$ mT.

Table 3
Summary of the Characteristics of Quartz and Feldspar Extracted From Core MD982187

Depth in core (m)	Mass fraction (wt%)	Carbonate-free mass fraction (wt%)	SIRM ($\times 10^{-3}$ Am^2/kg)	SIRM fraction (%)
6.34	18.7	27.9	3.63	24.1
7.38	19.4	22.4	7.85	35.0
11.32	12.8	19.9	3.43	25.9

Note. SIRM, saturation isothermal remanent magnetization.

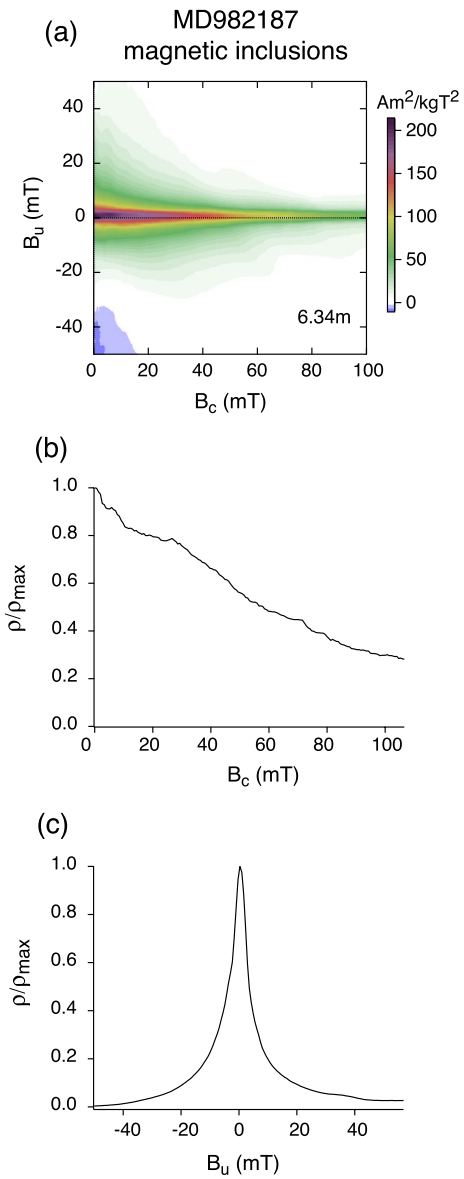

Figure 4. (a) Example of first-order reversal curve (FORC) diagrams of silicate-hosted magnetic inclusions extracted from Core MD982187, (b) horizontal profile along $B_u = 0$ mT of the FORC diagram, and (c) vertical profile along $B_c = 20$ mT.

interactions. The peak coercivity of the central ridge of each core is about 17 mT (KR0515-PC4), 12–18 mT (MD982187), and 22 mT (MR1402-PC1). FORC distributions with a broad vertical spread are also present, which indicates the contributions of interacting SD or vortex grains. They are probably of terrigenous origin, although magnetofossils may also contribute to the vertical spread when they deviate from a single intact chain arrangement like a collapsed chain. The contribution of the interacting component is the largest in Core KR0515-PC4, while it is the smallest in Core MR1402-PC1, as can be recognized from the vertical profiles in Figures 3m–3o. This will be quantified by PCA below. This is interpreted to reflect decreasing terrigenous inputs with increasing distance from New Guinea. Horizontal profiles along $B_u = 0$ show that the FORC distributions of Cores KR0515-PC4 and MD982187 extend to a higher coercivity range beyond 80 mT (Figures 3j and 3k). On the other hand, high coercivity tails are small in Core MR1402-PC1 compared with the former two cores (Figure 3l). It is also noted that Core MD982187 shows considerable within-core variations in peak coercivities and high-coercivity tails, whereas the variations are small in other two cores (Figures 3j–3l).

Quartz and feldspar as the residue of the chemical separation from Core MD982187 samples occupy ~13–19 weight percent of the original sediments, and carry ~24%–35% of SIRM (Table 3). Thus the sediments contain a significant amount of magnetic minerals as inclusions. The FORC diagrams of the residues show a relatively narrow peak elongated along the B_c axis, but the vertical spread is wider than the central ridge of untreated sediments (Figure 4). The vertical spread becomes wider with decreasing coercivity, which would represent a signature of weakly interacting particles (Egli, 2006). Some previous studies suggested from transmission electron microscopy that silicate-hosted magnetic inclusions are mainly in SD size (L. Chen et al., 2017) and have significant magnetostatic interactions (Zhang et al., 2018). The FORC distributions near the origin (Figure 4a) suggest that inclusions of super-paramagnetic (SP) or near the SP/SD boundary are abundant. The relatively small vertical spread of the residues suggests that magnetostatic interactions among inclusions may not be as strong as those of other terrigenous magnetic minerals. The horizontal profiles along $B_u = 0$ indicate FORC distributions extending to a high-coercivity range beyond 80 mT. Thus it is inferred that silicate-hosted magnetic inclusions carry partly, if not mostly, the higher-coercivity component observed in Cores KR0515-PC4 and MD982187.

PCA was applied to FORC diagrams (FORC-PCA) of the samples from the three cores and the chemical extracts from Core MD982187. First, the data points from all samples were plotted on a principal-component PC1-PC2 plane. The reliability of the data can be examined using the physical metrics of Harrison et al. (2018), which assess the feasibility of reconstructed FORCs from three criteria, saturation (nonexistence of a FORC exceeding the normalized value), monotonicity (nonnegative first derivative of a FORC with respect to the measurement field), and crossing (no intersection of individual FORCs), and the three metrics are combined into a single feasibility metric (Harrison et al., 2018). Samples with the feasibility metric of lower than 0.9 were excluded. The numbers of samples remained are 35, 34, and 11 for Cores KR0515-PC4, MD982187, and MR1402-PC1, respectively. All three samples of silicate-hosted magnetic inclusions passed the feasibility metric test. Low signal-to-noise ratios of

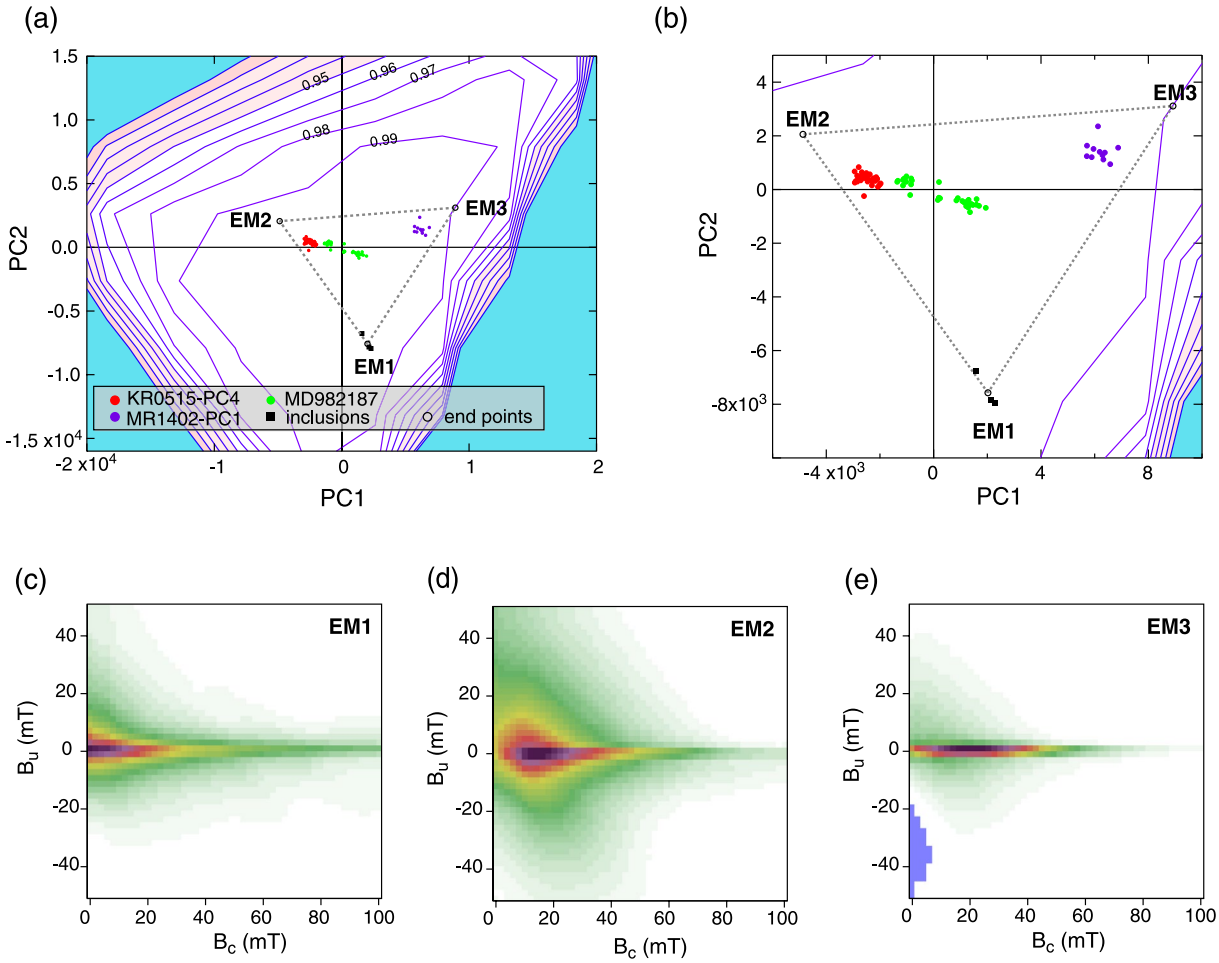

Figure 5. Results of principal component analysis applied to first-order reversal curve (FORC) diagrams from the three cores and silicate-hosted magnetic inclusions extracted from Core MD982187. (a) Distribution of FORC data on the principal component PC1-PC2 plane. Red: Core KR0515-PC4, green: MD982187, purple: MR1402-PC1, black: silicate-hosted magnetic inclusions extracted from Core MD982187. Triangular dashed lines define a three-endmember (EM) system. Contours represent the feasibility metric (Harrison et al., 2018). (b) Enlargement of panel (a). (c–e) FORC diagrams of EM1, EM2, and EM3, representing mainly silicate-hosted magnetic inclusions, other terrigenous magnetic minerals, and magnetofossils, respectively.

original FORC data due to weak magnetization are likely responsible for the low feasibility metrics, in particular for Core MR1402-PC1. Then PCA was conducted again using the remaining data (Figure 5). Data variance of ~92% can be explained by the two PCs (PC1: ~71%, PC2: ~21%). Three EMs (EM1, EM2, and EM3) were selected on the PC1-PC2 plane, and the contributions of individual EMs were calculated.

EM1 was selected close to the data points of the chemical extracts. We assume that EM1 reflects silicate-hosted magnetic inclusions. Although distance among silicates that host magnetic minerals in the extracts are different from those in the original sediments, this influence on the FORC diagrams is inferred to be small because magnetostatic interactions among magnetic inclusions within the same silicate host would be more significant than those among different silicates.

EM2 has an elliptical peak centered at B_c = ~15 mT on the B_u = 0 axis with a large vertical spread, and does not contain a central ridge (Figure 5d). EM2 bears the signature of interacting SD/vortex grains (Harrison et al., 2018; Muxworthy et al., 2004), and is interpreted to reflect terrigenous magnetic grains except for silicate-hosted magnetic inclusions. EM3 is dominated by the central ridge representing noninteracting SD grains, and considered to be carried mainly by magnetofossils (Figure 5e). The choice of EMs has some arbitrariness; EM2 and EM3 were selected so that the two EMs look distinct with each other and the component with a vertical spread in EM3 is as small as possible. The variations of the data from Core MD982187 are not parallel to the EM2-EM3 mixing line, but fall more in the middle of the space defined by the three EMs

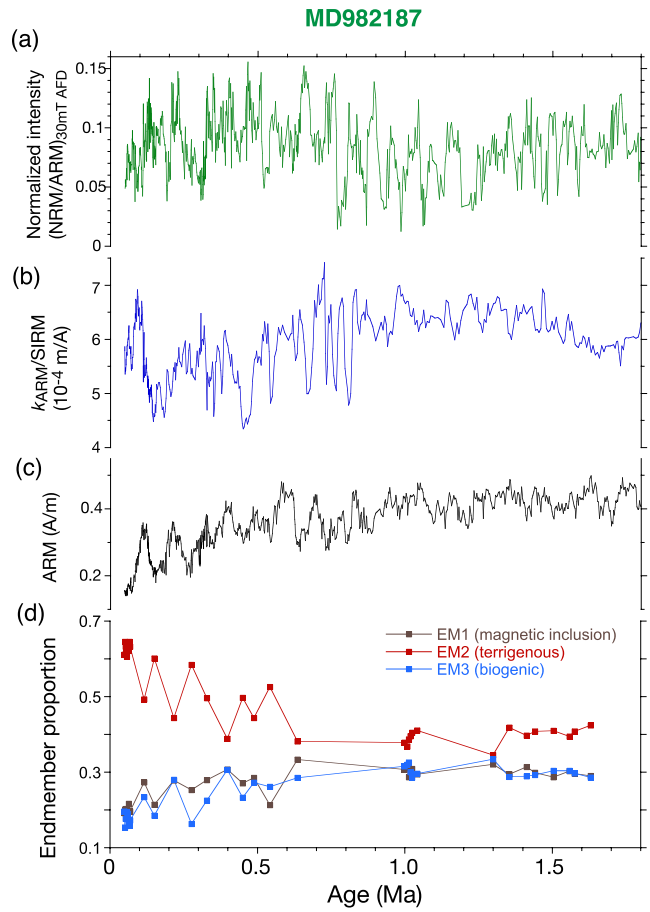

Figure 6. (a) Variations of relative paleointensity with age of Core MD982187 based on natural remanent magnetization (NRM) intensity normalized by anhysteretic remanent magnetizatio (ARM) intensity after alternating-field demagnetization at a peak field of 30 mT (Yamazaki & Oda, 2005), (b) ARM susceptibility to saturation isothermal remanent magnetization (k_{ARM}/SIRM) ratio (Tauxe & Yamazaki, 2015), (c) ARM intensity (Yamazaki & Oda, 2005), and (d) the proportions of endmember (EM)1 (gray), EM2 (red), and EM3 (blue).

(Figure 5b). This suggests that magnetic mineral assemblages of these three cores are not a simple mixture of two components like terrigenous versus magnetofossil, and supports the incorporation of another component representing silicate-hosted magnetic inclusions.

In Core KR0515-PC4, the proportion of EM1 (~20%) plus EM2 (~70%) accounts for about 90% of the magnetization, and EM3 accounts only about 10% (Table 2, Figure S1 in Supporting Information S1). Thus magnetic grains of this core are considered to be dominated (roughly 90%) by terrigenous magnetic minerals, although the proportion depends on the choice of EM positions on the PC1-PC2 plane. On the other hand, magnetofossils (EM3) explains ~70% of the magnetization of Core MR1402-PC1 (Table 2, Figure S2 in Supporting Information S1). Within-core variations of the PC scores are minor for Cores KR0515-PC4 and MR1402-PC1. On the other hand, the PC1 score shows some changes within Core MD982187 (Figures 5b and 6).

5. Discussion

The results of FORC-PCA indicated that there are large differences in the EM3 (magnetofossil) proportion among the three cores, ranging from 8.4% to 72.9%, and that the variations of the EM3 proportion parallel to the k_{ARM}/SIRM ratio (Table 2). This confirms that the k_{ARM}/SIRM ratio reflects the proportion of magnetofossils to terrigenous magnetic minerals in this region. The average normalized intensity (NRM/ARM)

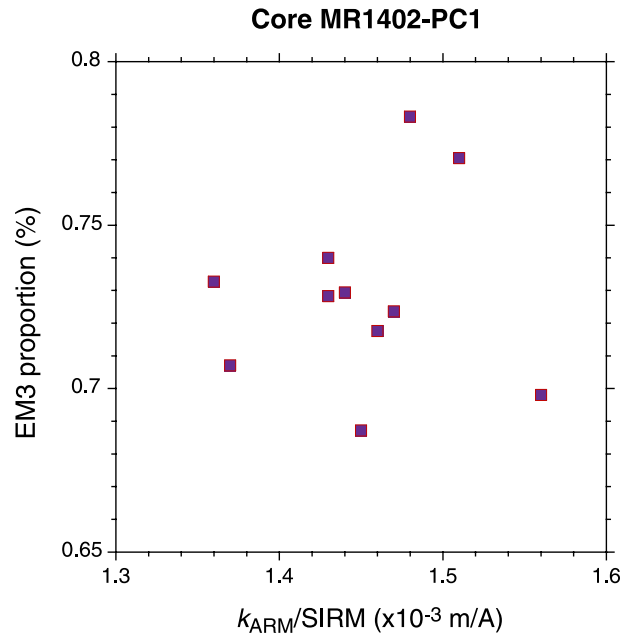

Figure 7. Relation between the anhysteretic remanent magnetization susceptibility to saturation isothermal remanent magnetization (k_{ARM}/SIRM) ratio and the proportion of endmember (EM)3 in Core MR1402-PC1. EM3 represents mainly of magnetofossils, which was derived from first-order reversal curve-principal component analysis shown in Figure 5.

decreases with increasing EM3 proportion (Table 2). Core MD982187 shows within-core variations of the EM3 proportion (Figure 6). These variations parallel to the k_{ARM}/SIRM ratio, and the peaks in EM3 and the k_{ARM}/SIRM ratio broadly correspond to lows in NRM/ARM. These observations indicate that RPI normalized by ARM is influenced by the relative abundance of magnetofossils in sediments, and that underestimation of RPI occurs in sediments with increasing proportion of magnetofossils. This is probably because ARM acquisition efficiency of magnetofossils is higher compared with those of terrigenous magnetic minerals due to small magnetostatic interactions. NRM acquisition might also be influenced by the strength of magnetostatic interactions, but the dependency on magnetostatic interactions for ARM acquisition would be larger than that for NRM, and hence ARM fails to compensate for NRM acquisition efficiency changes caused by variations in the abundance of magnetofossils. ARM is thus not an appropriate normalizer of RPI estimations for sediments with variable amounts of magnetofossils.

FORC-PCA applied to samples from all three cores showed a large proportion of EM3 (~70%) for Core MR1402-PC1, which indicates that magnetic mineral assemblages in this core are dominated by magnetofossils. Variations in the proportion of the biogenic (EM3) to terrigenous components (EM1 plus EM2) within this core are small, whereas the k_{ARM}/SIRM ratio varies (Figures 2, 5b and S2 in Supporting Information S1). Furthermore, the EM3 proportion does not correlate with the k_{ARM}/SIRM ratio (Figures 7 and S2 in Supporting Information S1). These observations suggest that the variations of the k_{ARM}/SIRM ratio in this core are induced by a factor other than the proportion of magnetofossils to terrigenous magnetic minerals.

In order to investigate the cause of k_{ARM}/SIRM ratio changes, we conducted FORC-PCA using only the samples from Core MR1402-PC1 (Figure 8). All 23 FORC diagrams measured on this core were used for PCA, and no selection based on the feasibility metric was applied although signal-to-noise ratios of the samples are generally low due to weak magnetization. PC1 and PC2 explain ~33% and 22%, respectively, of the data variance. The k_{ARM}/SIRM ratio inversely correlates with the PC1 score, but does not show correlation with the PC2 score (Figure 8b). When comparing reconstructed FORC diagrams at PC scores (2,000, 0) and (−2,000, 0), the contribution of the central ridge component is smaller at (2,000, 0), whereas a broad background component is a little larger there (Figure 8a). The absence of correlation between the EM3 proportion and the k_{ARM}/SIRM ratio (Figure 7) suggests that the difference in the FORC diagrams may not be attributable to the increased terrigenous component. We speculate that increased magnetostatic

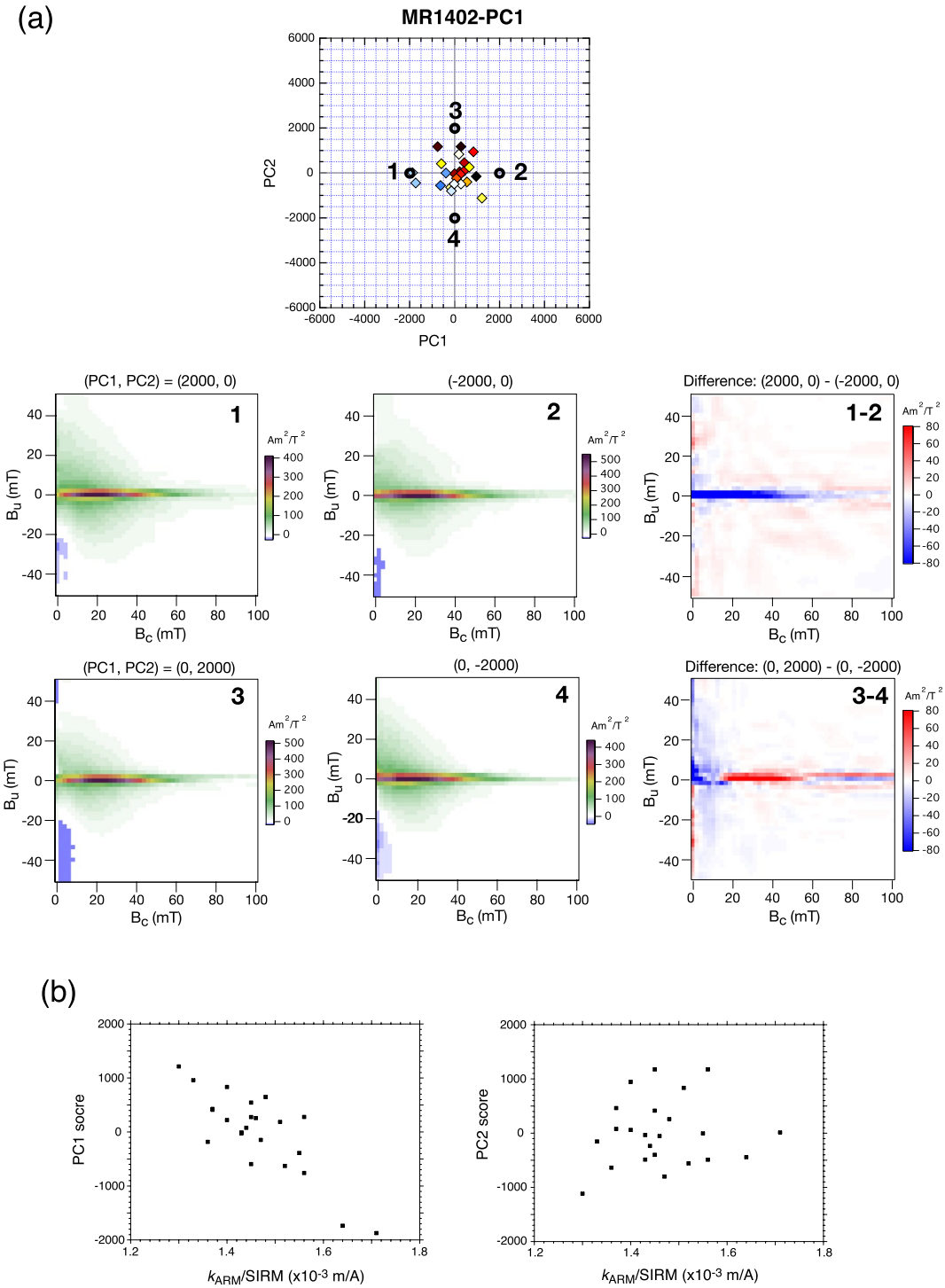

Figure 8. (a) Result of principal component analysis applied to first-order reversal curve (FORC) diagrams from Core MR1402-PC1. Diamonds show the distribution of FORC data on the PC1-PC2 plane. Reconstructed FORC diagrams at the positions 1 through 4 (circles) on the PC1-PC2 plane and the difference of the FORC diagrams between the position 1 (2,000, 0) and 2 (−2,000, 0) (the latter was subtracted from the former), and between the position 3 (0, 2,000) and 4 (0, −2,000) are presented. (b) Relation between the anhysteretic remanent magnetization susceptibility to saturation isothermal remanent magnetization (k_{ARM}/SIRM) ratio and PC1 (left) and PC2 (right) scores.

interactions due to bending and collapse of biogenic magnetite chains may be responsible for the increased background component and lower k_{ARM}/SIRM ratio (Chang et al., 2019; Li et al., 2012). Because magnetofossils dominate magnetic mineral assemblages in this core, the k_{ARM}/SIRM ratio may be affected by biogenic magnetite chain configurations rather than the proportion of magnetofossils to terrigenous magnetic minerals. As RPI normalized by ARM decreases with increasing k_{ARM}/SIRM ratios in this core as well (Figure 2a) (Sakuramoto et al., 2017), biogenic magnetite chain configurations may have influenced the RPI estimations. In addition, the comparison of the reconstructed FORC diagrams at PC scores (0, 2,000) and (0, −2,000) suggests that the contributions of extremely low coercivity near the origin increase with lower PC2 scores. These might represent nonchained isolated magnetofossils (Usui & Yamazaki, 2021). On the other hand, the contributions of the broad background component are similar (Figure 8a), which may explain the absence of the correlation between the k_{ARM}/SIRM ratio and the PC2 score (Figure 8b).

The fraction of SIRM carried by the terrigenous components was estimated for each core from the sum of the EM1 and EM2 proportions and total SIRM: 5.79 A/m in average for Core KR0515-PC4, 5.89 A/m for MD982187, and 0.54 A/m for MR1402-PC1. When the differences of the sedimentation rates are taken into account (Table 1), terrigenous magnetic flux is the largest at Core KR0515-PC4 and decreases with the distance from New Guinea as expected. This supports that terrigenous particles in this region are mainly of fluvial origin from the Sepik River in New Guinea. In Core MD982187, the proportion of EM1 ranges from ∼20% to 30% (Figure 6d), which is consistent with the observation that silicate-hosted magnetic inclusions extracted from Core MD982187 carry ∼24% to 35% of SIRM (Table 3).

The contribution of silicate-hosted magnetic inclusions to the total magnetization of Core MD982187 is much larger than that of pelagic red clay in the South Pacific, ∼1% of SIRM (Usui et al., 2018). The mass fraction of quartz and feldspar contained in Core MD982187, ∼20% to 28% in carbonate free basis (Table 3), is a little larger than that in the red clay, reported as 2.3%–22.7%. The concentration of magnetic minerals embedded in host silicates seems to be larger in the studied sediments than the red clay, 3.4–7.9 versus $0.7–2.0 \times 10^{-3}$ Am^2/kg as SIRM (Usui et al., 2018), which would reflect differences of source rocks. But these two factors may not be sufficient for explaining the difference in the contribution of silicate-hosted magnetic inclusions to the total magnetization. This suggests that pelagic red clay may contain a larger amount of unprotected magnetic minerals, which may be attached to clay minerals. Our FORC-PCA revealed that the proportion of the magnetization carried by inclusions (EM1) to the magnetization by other terrigenous magnetic minerals (EM2) changes according to the distance from New Guinea; the EM1 proportion is significantly smaller than EM2 in near-shore Core KR0515-PC4, whereas the two are comparable in Core MR1402-PC1 (Figure 5), which is the farthest from New Guinea. This suggests that silicate-hosted magnetic inclusions may be transported for longer distances in this region, whereas unprotected magnetic minerals may deposit earlier.

In this study, we have discussed the influence of the proportional variations of magnetofossils in magnetic mineral assemblages on RPI estimations. For reliable RPI estimations, such influence should be corrected for. To achieve this, it is necessary to understand the differences of magnetization acquisition efficiency of NRM and the normalizes between magnetofossils and terrigenous magnetic minerals in sediments. Furthermore, PCA of the FORC diagrams suggested that the system is not a two-component mixture of magnetofossil and terrigenous magnetic minerals, but that silicate-hosted magnetic inclusions and other terrigenous magnetic minerals may behave differently. Core MD982187 has a larger proportion of EM1 to EM2 compared with that of Core KR0515-PC4 (Figures 6 and S1 in Supporting Information S1). This difference may be related to the observation that Core MD982187 has NRM/IRM values nearly as small as these of Core MR1402-PC1 although its NRM/ARMs are nearly as large as those of Core KR0515-PC4 (Figure 2). Further studies are needed to understand the behavior of individual magnetic constituents for reliable RPI estimations.

6. Conclusions

FORC-PCA was applied on three sediment cores from the western equatorial Pacific, among which average RPI normalized by ARM and the k_{ARM}/SIRM ratio differ significantly. Magnetic mineral assemblages in Core KR0515-PC4 are dominated (∼90%) by terrigenous magnetic minerals of likely fluvial origin from

New Guinea. Magnetic grains in Core MD982187 are a mixture of magnetofossils and terrigenous magnetic minerals, and magnetic mineral inclusions hosted by quartz and feldspar carry about 30% of the magnetization. Core MR1402-PC1 is dominated by magnetofossils (~70%). RPI based on NRM/ARM decreases with increasing proportion of magnetofossils. This is probably due to that ARM acquisition efficiency of the magnetofossil component is higher compared with the terrigenous magnetic component due to small magnetostatic interactions. The k_{ARM}/SIRM ratio generally increases with increasing magnetofossil component in FORC-PCA. Within Core MR1402-PC1, however, the k_{ARM}/SIRM ratio changes significantly despite little variation in the proportion of magnetofossils. Bending and collapse of biogenic magnetite chains may also influence the k_{ARM}/SIRM ratio and RPI estimations.

Data Availability Statement

FORC data produced in this study are available in Zenodo repository (https://doi.org/10.5281/zenodo.5148028).

Acknowledgments
The authors thank Yoshuke Miyairi for the help of part of the chemical separation of quartz and feldspar, and Juichiro Ashi for valuable suggestions. The manuscript was greatly improved by constructive review comments from Ioan Lascu and Ramon Egli. This study is partly supported by JSPS KAKENHI Grant Number 19H01997.

References

Banerjee, S. K., King, J., & Marvin, J. (1981). A rapid method for magnetic granulometry with applications to environmental studies. *Geophysical Research Letters*, *8*, 333–336. https://doi.org/10.1029/gl008i004p00333

Berndt, T. A., Chang, L., & Pei, Z. (2020). Mind the gap: Towards a biogenic magnetite paleoenvironmental proxy through an extensive finite-element micromagnetic simulation. *Earth and Planetary Science Letters*, *532*, 116010. https://doi.org/10.1016/j.epsl.2019.116010

Blatt, H., Jones, R. L., & Charles, R. G. (1982). Separation of quartz and feldspars from mudrocks. *Journal of Sedimentary Research*, *52*(2), 660–661. https://doi.org/10.2110/jsr.52.660

Chang, L., Harrison, R. J., & Berndt, T. A. (2019). Micromagnetic simulation of magnetofossils with realistic size and shape distributions: Linking magnetic proxies with nanoscale observations and implications for magnetofossil identification. *Earth and Planetary Science Letters*, *527*, 115790. https://doi.org/10.1016/j.epsl.2019.115790

Chang, L., Roberts, A. P., Heslop, D., Hayashida, A., Li, J., Zhao, X., et al. (2016). Widespread occurrence of silicate-hosted magnetic mineral inclusions in marine sediments and their contribution to paleomagnetic recording. *Journal of Geophysical Research: Solid Earth*, *121*, 8415–8431. https://doi.org/10.1002/2016JB013109

Chang, L., Roberts, A. P., Winklhofer, M., Heslop, D., Dekkers, M. J., Krigsman, W., et al. (2014). Magnetic detection and characterization of biogenic magnetic minerals: A comparison of ferromagnetic resonance and first-order reversal curve diagrams. *Journal of Geophysical Research: Solid Earth*, *119*, 6136–6158. https://doi.org/10.1002/2014JB011213

Channell, J. E. T., Harrison, R. J., Lascu, I., McCave, I. N., Hibbert, F. D., & Austin, W. E. N. (2016). Magnetic record of deglaciation using FORC-PCA, sortable-silt grain size, and magnetic excursion at 26 ka, from the Rockall Trough (NE Atlantic). *Geochemistry, Geophysics, Geosystems*, *17*, 1823–1841. https://doi.org/10.1002/2016GC006300

Channell, J. E. T., Xuan, C., & Hodell, D. A. (2009). Stacking paleointensity and oxygen isotope data for the last 1.5 Myr (PISO-1500). *Earth and Planetary Science Letters*, *283*, 14–23. https://doi.org/10.1016/j.epsl.2009.03.012

Chen, A. P., Egli, R., & Moskowitz, B. M. (2007). First-order reversal curve (FORC) diagrams of natural and cultured biogenic magnetic particles. *Journal of Geophysical Research*, *112*, B08S90. https://doi.org/10.1029/2006jb004575

Chen, L., Heslop, D., Roberts, A. P., Chang, L., Zhao, X., McGregor, H. V., et al. (2017). Remanence acquisition efficiency in biogenic and detrital magnetite and recording of geomagnetic paleointensity. *Geochemistry, Geophysics, Geosystems*, *18*, 1435–1450. https://doi.org/10.1002/2016GC006753

Clayton, R. N., Rex, R. W., Syers, J. K., & Jackson, M. L. (1972). Oxygen isotope abundance in quartz from Pacific pelagic sediments. *Journal of Geophysical Research*, *77*(21), 3907–3915. https://doi.org/10.1029/JC077i021p03907

Dang, H., Wu, J., Xiong, Z., Qiao, P., Li, T., & Jian, Z. (2020). Orbital and sea-level changes regulate the iron-associated sediment supplies from Papua New Guinea to the equatorial Pacific. *Quaternary Science Reviews*, *239*, 106361. https://doi.org/10.1016/j.quascirev.2020.106361

Egli, R. (2004). Characterization of individual rock magnetic components by analysis of remanence curves. 2. Fundamental properties of coercivity distributions. *Physics and Chemistry of the Earth*, *29*, 851–867. https://doi.org/10.1016/s1474-7065(04)00129-9

Egli, R. (2006). Theoretical aspects of dipolar interactions and their appearance in first-order reversal curves of thermally activated single-domain particles. *Journal of Geophysical Research*, *111*, B12S17. https://doi.org/10.1029/2006jb004567

Egli, R. (2013). VARIFORC: An optimized protocol for calculating non-regular first-order reversal curve (FORC) diagrams. *Global and Planetary Change*, *110*, 302–320. https://doi.org/10.1016/j.gloplacha.2013.08.003

Egli, R., Chen, A. P., Winklhofer, M., Kodama, K. P., & Horng, C. S. (2010). Detection of noninteracting single domain particles using first-order reversal curve diagrams. *Geochemistry, Geophysics, Geosystems*, *11*, Q01Z11. https://doi.org/10.1029/2009GC002916

Harrison, R. J., & Feinberg, J. M. (2008). FORCinel: An improved algorithm for calculating first-order reversal curve distributions using locally weighted regression smoothing. *Geochemistry, Geophysics, Geosystems*, *9*, Q05016. https://doi.org/10.1029/2008GC001987

Harrison, R. J., Muraszko, J., Heslop, D., Lascu, I., Muxworthy, A. R., & Roberts, A. P. (2018). An improved algorithm for unmixing first-order reversal curve diagrams using principal component analysis. *Geochemistry, Geophysics, Geosystems*, *19*, 1595–1610. https://doi.org/10.1029/2018gc007511

Hoffmann, D. I., & Fabian, K. (2009). Correcting relative paleointensity records for variations in sediment composition: Results from a South Atlantic stratigraphic network. *Earth and Planetary Science Letters*, *284*, 34–43. https://doi.org/10.1016/j.epsl.2009.03.043

Johnson, E. A., Murphy, T., & Torreson, O. W. (1948). Pre-history of the Earth's magnetic field. *Terrestrial Magnetism and Atmospheric Electricity*, *53*, 349–372. https://doi.org/10.1029/te053i004p00349

King, J., Banerjee, S. K., Marvin, J., & Özdemir, Ö. (1982). A comparison of different magnetic methods for determining the relative grain size of magnetite in natural materials: Some results from lake sediments. *Earth and Planetary Science Letters*, *59*, 404–419. https://doi.org/10.1016/0012-821x(82)90142-x

King, J. W., Banerjee, S. K., & Marvin, J. (1983). A new rock magnetic approach to selecting sediments for geomagnetic paleointensity studies: Application to paleointensity for the last 4000 years. *Journal of Geophysical Research*, *88*, 5911–5921. https://doi.org/10.1029/jb088ib07p05911

Lascu, I., Harrison, R. J., Li, Y., Muraszko, J. R., Channell, J. E. T., Piotrowski, A. M., & Hodell, D. A. (2015). Magnetic unmixing of first-order reversal curve diagrams using principal component analysis. *Geochemistry, Geophysics, Geosystems*, *16*, 2900–2915. https://doi.org/10.1002/2015gc005909

Levi, S., & Banerjee, S. K. (1976). On the possibility of obtaining relative paleointensities from lake sediments. *Earth and Planetary Science Letters*, *29*, 219–226. https://doi.org/10.1016/0012-821x(76)90042-x

Li, J., Wu, W., Liu, Q., & Pan, Y. (2012). Magnetic anisotropy, magnetostatic interactions and identification of magnetofossils. *Geochemistry, Geophysics, Geosystems*, *13*, Q10Z51. https://doi.org/10.1029/2012GC004384

Muxworthy, A., Heslop, D., & Williams, W. (2004). Influence of magnetostatic interactions on first-order-reversal-curve (FORC) diagrams: A micromagnetic approach. *Geophysical Journal International*, *158*, 888–897. https://doi.org/10.1111/j.1365-246x.2004.02358.x

Pike, C. R., Roberts, A. P., & Verosub, K. L. (1999). Characterizing interactions in fine magnetic particle systems using first order reversal curves. *Journal of Applied Physics*, *85*(9), 6660–6667. https://doi.org/10.1063/1.370176

Rea, D. K. (1994). The paleoclimatic record provided by eolian deposition in the deep sea: The geologic history of wind. *Reviews of Geophysics*, *32*, 159–195. https://doi.org/10.1029/93rg03257

Roberts, A. P., Chang, L., Heslop, D., Florindo, F., & Larrasoaña, J. C. (2012). Searching for single domain magnetite in the "pseudo-single domain" sedimentary haystack: Implications of biogenic magnetite preservation for sediment magnetism and relative paleointensity determinations. *Journal of Geophysical Research*, *117*, B08104. https://doi.org/10.1029/2012JB009412

Roberts, A. P., Florindo, F., Villa, G., Chang, L., Jovane, L., Bohaty, S. M., et al. (2011). Magnetotactic bacterial abundance in pelagic marine environments is limited by organic carbon flux and availability of dissolved iron. *Earth and Planetary Science Letters*, *310*, 441–452. https://doi.org/10.1016/j.epsl.2011.08.011

Roberts, A. P., Heslop, D., Zhao, X., & Pike, C. R. (2014). Understanding fine magnetic particle systems through use of first-order reversal curve diagrams. *Reviews of Geophysics*, *52*, 557–602. https://doi.org/10.1002/2014RG000462

Roberts, A. P., Pike, C. R., & Verosub, K. L. (2000). First-order reversal curve diagrams: A new tool for characterizing the magnetic properties of natural samples. *Journal of Geophysical Research*, *105*, 461–475. https://doi.org/10.1029/2000jb900326

Roberts, A. P., Zhao, X., Harrison, R. J., Heslop, D., Muxworthy, A. R., Rowan, C. J., et al. (2018). Signatures of reductive magnetic mineral diagenesis from unmixing of first-order reversal curves. *Journal of Geophysical Research: Solid Earth*, *123*, 4500–4522. https://doi.org/10.1029/2018JB015706

Sakuramoto, Y., Yamazaki, T., Kimoto, K., Miyairi, Y., Kuroda, J., Yokoyama, Y., & Matsuzaki, H. (2017). A geomagnetic paleointensity record of 0.6 to 3.2 Ma from sediments in the western equatorial Pacific and remanent magnetization lock-in depth. *Journal of Geophysical Research: Solid Earth*, *122*, 7525–7543. https://doi.org/10.1002/2017jb014450

Stevens, R. L. (1991). Grain-size distribution of quartz and feldspar extracts and implications for flocculation processes. *Geo-Marine Letters*, *11*(3–4), 162–165. https://doi.org/10.1007/bf02431004

Syers, J. K., Chapman, S. L., Jackson, M. L., Rex, R. W., & Clayton, R. N. (1968). Quartz isolation from rocks, sediments and soils for determination of oxygen isotopes composition. *Geochimica et Cosmochimica Acta*, *32*(9), 1022–1025. https://doi.org/10.1016/0016-7037(68)90067-7

Tauxe, L. (1993). Sedimentary records of relative paleointensity of the geomagnetic field: Theory and practice. *Reviews of Geophysics*, *31*, 319–354. https://doi.org/10.1029/93rg01771

Tauxe, L., & Yamazaki, T. (2015). Paleointensities. In G. Schubert (Ed.), Treatise on geophysics (2nd ed., Vol. 5, pp. 461–509). Elsevier. https://doi.org/10.1016/b978-0-444-53802-4.00107-x

Usui, Y., Shimono, T., & Yamazaki, T. (2018). Rock magnetism of quartz and feldspars chemically separated from pelagic red clay: A new approach to provenance study. *Earth, Planets and Space*, *70*, 133. https://doi.org/10.1186/s40623-018-0918-1

Usui, Y., & Yamazaki, T. (2021). Non-chained, non-interacting, stable single-domain maghemite octahedra in deep-sea red clay: A new type of magnetofossil? *Geochemistry, Geophysics, Geosystems*, *22*, e2021GC009770. https://doi.org/10.1029/2021GC009770

Wagner, C. L., Lascu, I., Lippert, P. C., Egli, R., Livi, K. J. T., & Sears, H. B. (2021). Diversification of iron-biomineralizing organisms during the Paleocene-Eocene Thermal Maximum: Evidence from quantitative unmixing of magnetic signatures of conventional and giant magnetofossils. *Paleoceanography and Paleoclimatology*, *36*, e2021PA004225. https://doi.org/10.1029/2021PA004225

Winckler, G., Anderson, R. F., Jaccard, S. L., & Marcantonio, F. (2016). Ocean dynamics, not dust, have controlled equatorial Pacific productivity over the past 500,000 years. *Proceedings of the National Academy of Sciences*, *113*(22), 6119–6124. https://doi.org/10.1073/pnas.1600616113

Wu, J., Liu, Z., & Zhou, C. (2013). Provenance and supply of Fe-enriched terrigenous sediments in the western equatorial Pacific and their relation to precipitation variations during the late Quaternary. *Global and Planetary Change*, *108*, 56–71. https://doi.org/10.1016/j.gloplacha.2013.06.002

Yamazaki, T. (2008). Magnetostatic interactions in deep-sea sediments inferred from first-order reversal curve diagrams: Implications for relative paleointensity normalization. *Geochemistry, Geophysics, Geosystems*, *9*, Q02005. https://doi.org/10.1029/2007GC001797

Yamazaki, T. (2017). *DRM lock-in depth and magnetofossils*. Paper presented at International Conference on Rock Magnetism 2017.

Yamazaki, T., Fu, W., Shimono, T., & Usui, Y. (2020). Unmixing biogenic and terrigenous magnetic mineral components in red clay of the Pacific Ocean using principal component analyses of first--order reversal curve diagrams and paleoenvironmental implications. *Earth, Planets and Space*, *72*, 120. https://doi.org/10.1186/s40623-020-01248-5

Yamazaki, T., & Horiuchi, K. (2016). Precessional control on ocean productivity in the Western Pacific Warm Pool for the last 400 kyr: Insight from biogenic magnetite. *Geochemistry, Geophysics, Geosystems*, *17*, 4399–4412. https://doi.org/10.1002/2016GC006446

Yamazaki, T., & Ikehara, M. (2012). Origin of magnetic mineral concentration variation in the Southern Ocean. *Paleoceanography*, *27*, PA2206. https://doi.org/10.1029/2011PA002271

Yamazaki, T., Kanamatsu, T., Mizuno, S., Hokanishi, N., & Gaffar, E. Z. (2008). Geomagnetic field variations during the last 400 kyr in the western equatorial Pacific: Paleointensity-inclination correlation revisited. *Geophysical Research Letters*, *35*, L20307. https://doi.org/10.1029/2008GL035373

Yamazaki, T., & Oda, H. (2005). A geomagnetic paleointensity stack between 0.8 and 3.0 Ma from equatorial Pacific sediment cores. *Geochemistry, Geophysics, Geosystems*, *6*, Q11H20. https://doi.org/10.1029/2005GC001001

Yamazaki, T., & Shimono, T. (2013). Abundant bacterial magnetite occurrence in oxic red clay. *Geology*, *41*, 1191–1194. https://doi.org/10.1130/g34782.1

Yamazaki, T., & Yamamoto, Y. (2018). Relative paleointensity and inclination anomaly over the last 8 Myr obtained from the Integrated Ocean Drilling Program Site U1335 sediments in the eastern equatorial Pacific. *Journal of Geophysical Research: Solid Earth*, *123*, 7305–7320. https://doi.org/10.1029/2018JB016209

Yamazaki, T., Yamamoto, Y., Acton, G., Guidry, E. P., & Richter, C. (2013). Rock-magnetic artifacts on long-term relative paleointensity variations in sediments. *Geochemistry, Geophysics, Geosystems*, *14*, 29–43. https://doi.org/10.1002/ggge.20064

Zhang, Q., Liu, Q., Li, J., & Sun, Y. (2018). An integrated study of the eolian dust in pelagic sediments from the North Pacific Ocean based on environmental magnetism, transmission electron microscopy, and diffuse reflectance spectroscopy. *Journal of Geophysical Research: Solid Earth*, *123*, 3358–3376. https://doi.org/10.1002/2017JB014951